

# Extension and validation of a revised Cassie-Baxter model for tailor-made surface topography design and controlled wettability

Nikolaos Lempesis,<sup>1,2,\*</sup> Rudolf J. Koopmans,<sup>1,2</sup> Ruth Díez-Ahedo<sup>3</sup>, Per Magnus Kristiansen<sup>4,5,6</sup>

<sup>1</sup>*Plastics Innovation Competence Center, Passage du Cardinal 1, CH-1700 Fribourg, Switzerland*

<sup>2</sup>*Department of Mechanical Engineering, College of Engineering and Architecture Fribourg HES-SO, Bd de Pérolles 80, CH-1705 Fribourg, Switzerland*

<sup>3</sup>*Tekniker, Iñaki Goenaga 5, 20600 Eibar, Spain*

<sup>4</sup>*FHNW University of Applied Sciences and Arts Northwestern Switzerland, School of Engineering, Institute of Polymer Nanotechnology (INKA), Klosterzelgstrasse 2, CH-5210 Windisch, Switzerland*

<sup>5</sup>*Laboratory for Micro- and Nanotechnology, Paul Scherrer Institute, 5232 Villigen PSI, Switzerland*

<sup>6</sup>*University College Dublin, School of Mechanical and Material Engineering, Belfield, Dublin 4, Ireland*

<sup>\*</sup>**Author to whom correspondence should be addressed:** [nikolaos.lempesis@hefr.ch](mailto:nikolaos.lempesis@hefr.ch)

**Keywords:** wettability, wetting model, topography, Cassie-Baxter, hydrophobic, omniphobic

## Abstract

Predicting wettability accurately across various materials, surface topographies and wetting liquids is undeniably of paramount importance as it sets the foundations for technological developments related to improved life quality, energy saving and economization of resources, thereby reducing the environmental impact for recycling and reuse. In this work, we extend and validate our recently published wetting model, constituting a refinement of the original Cassie-Baxter model after consideration of realistic curved liquid-air interfaces. Our model enabled more meaningful contact angle predictions, while it captured the experimentally observed trends between contact angle and surface roughness. Here, the formalism of our

wetting model is further extended to 3D surface topographies, whereas the validity of our model, in its entirety, is evaluated. To this end, a total of thirty-two experimentally engineered surfaces of various materials exhibiting single- and multilevel hierarchical topographies of increasing complexity were utilized. Our model predictions were consistently in remarkable agreement with experimental data (deviations of 3-6%) and, in most cases, within statistical inaccuracies of the experimental measurements. Direct comparison between experiments and modeling results corroborated that surface topographies featuring re-entrant geometries promoted enhanced liquid-repellency, whereas hierarchical multilevel surface topographies enabled even more pronounced nonwetting behaviors. For the sinusoidal topography, consideration of a second superimposing topography level almost doubled the observed water contact angles, whereas addition of a third level brought about an extra 12.5% increase in water contact angle.

## 1. Introduction

Everyday life commodities, such as food, water and other beverages, as well as inedible domestic products, such as cosmetics and liquid detergents are stored, transported and maintained within plastic or glassy containers. Adhesion of these goods to their packaging material is responsible for product waste [1], poor product appearance [2], increased package recycling costs [3], as well as sanitary problems and production deterioration in industrial units due to fouling of equipment [4]. Wettability was identified as the most dominant mechanism related to adhesion of a liquid onto a solid surface. This mechanism described the interactions between a liquid and a solid surface and was quantified, at mechanical equilibrium, by means of the apparent contact angle  $\theta$ , also referred to as static contact angle [5]. Liquid-repellent surfaces exhibited increased resistance to wetting which translated into large values for  $\theta$ . Controlling wettability of a surface proved to be a valuable tool for the design of numerous engineering applications including hydrophobic [6, 7] or oleophobic [8] non-wetting textiles, anti-fogging [9] and anti-icing [10] technologies, optimized buoyancy [11] and associated flow improvement [12], as well as antibiofouling [13] and water collection from fog [14].

Despite numerous applications invoking the theoretical underpinnings of wettability, understanding and controlling it remains largely still elusive thereby constituting a perpetual struggle for scientist, in which, luckily, they are not alone. To the observant enough and with keen perceptiveness, nature proved to be a valuable ally exemplifying numerous cases of

1  
2  
3 biological surfaces with remarkable wetting behavior. In the relatively recently spawned and  
4 rapidly developing fields of biomimetics and bionics, applications were engineered with  
5 functions emulating everyday behavior of such biological systems. Prominent examples of  
6 such influential bioinspired-surfaces and resulting technological applications included non-  
7 reflective surfaces utilizing the “moth-eye” effect [15], inspection robots with highly adhesive  
8 surfaces making use of the “gecko-effect” [16, 17], self-cleaning window panes using the “lotus  
9 leaf effect” [18], solid bodies exhibiting improved flowability owed to reduced drag by  
10 exploiting the “shark skin effect” [19, 20], as well as numerous other emerging applications  
11 related to energy conversion and conservation [21].

12  
13  
14  
15  
16  
17  
18  
19 The difficulty to comprehend wettability fully was, in large part, attributed to the great number  
20 of parameters contributing to the intricacy of the phenomenon, including surface chemistry  
21 [22, 23], surface roughness [24, 25], temperature [26], mechanical loading [27], crystallinity  
22 [28] and applied electric field [29, 30]. Chemistry modifications of the surface, albeit  
23 promising, proved to have rather limited effect on wettability [31]. In contrast, changes in the  
24 surface topography appeared a more efficient way for manipulating wettability, even for the  
25 design of oil-repellent surfaces [32]. For even more pronounced control over wettability, very  
26 recently, topography modifications were combined efficiently with chemical treatment of  
27 various surfaces including cotton [33, 34], steel [35] and synthetic leather [36]. Further  
28 examples include trichloro(1H,1H,2H,2H-perfluorooctyl) silane (PFOCTS)-modified cobalt  
29 structures for creating omniphobic surfaces [37], Cd-Si co-doped TiO<sub>2</sub> thin films examining  
30 the synergistic effect of co-dopants and calcination temperature on wettability [38], as well as  
31 polymer nanocomposite surfaces comprising Au/ZnO nanoparticles randomly dispersed in a  
32 cellulose acetate polymer matrix [39]. A detailed compilation of substrate coatings and  
33 associated fabrication techniques can be found in the comprehensive work of B. Bhushan and  
34 S. Martin [40].

35  
36  
37  
38  
39  
40  
41  
42  
43  
44  
45  
46  
47  
48 In the general context of tinkering surface topography, surface roughness was of paramount  
49 importance [32, 41]. Extensive studies on biological surfaces, such as the leaves of *Ginkgo*  
50 *biloba* [25] and *Nelumbo nucifera* (lotus) [42] plants elaborated on the effect of roughness on  
51 overall nonwetting capabilities. The superhydrophobic traits of these biological surfaces were  
52 attributed initially to their distinct surface roughness which theoretically rendered them in a  
53 metastable state. This assumption was later on confirmed in the pioneering works of Marmur  
54 [43] and Nosonovsky [44]. Subsequently, an analysis entailing Gibbs surface free energy  
55 minimization in various solid-liquid-air systems showed that wetting states were distinct and  
56  
57  
58  
59  
60

1  
2  
3 could indeed be metastable and rather long-lived [45]. Besides surface roughness, biological  
4 surfaces often exhibited hierarchical organization, i.e., multiple levels of surface topographies  
5 placed on top of each other, which, in turn, was responsible for increased surface roughness  
6 owed to larger surface-to-volume ratio. A characteristic example was the morphology of the  
7 lotus leaves comprising nanoscale roughness superimposed over microscale bumps [46].  
8 Hierarchical topographies in biological surfaces were, in many instances, identified to promote  
9 liquid repellency [47, 48].

10  
11  
12  
13  
14  
15  
16 Engineered surfaces, on the other hand, differed, in many cases considerably, from biological  
17 surfaces due to multilevel hierarchical organization customarily present in the latter. This was  
18 because implementing multilevel topographies of multiplicity larger than two on engineered  
19 surfaces constituted a formidable technological challenge. Interestingly, non-hierarchical  
20 surfaces, which, however, retained some degree of roughness, displayed superhydrophobicity  
21 [49]. In addition, water-repelling surfaces were produced without necessarily featuring  
22 hierarchical topography [50, 51]. Therefore, in total, roughness was seemingly more important  
23 than hierarchical organization (multilevel topography), the latter being, however, beneficial for  
24 enhanced liquid-repellency.

25  
26  
27  
28  
29  
30  
31  
32 Modelling wettability played a decisive role in the design of surface topographies with tailored  
33 properties, as well as in the interpretation of experimental observations. Ever since the  
34 inaugural modelling attempts undertaken by Thomas Young in 1805 [52], followed by Wenzel  
35 [53] and eventually by Cassie and Baxter [54], numerous theoretical works emerged [55-60]  
36 thereby manifesting the great technological potential associated with increased wettability  
37 control. Without any loss of generality and for simplicity, most of these models considered  
38 only two-dimensional (2D) systems, implying that the surface texture extended to infinity along  
39 the remaining dimension forming thus a semi-infinite three-dimensional (3D) representation.  
40 This practice was customary and was shown to produce results in gratifying agreement with  
41 realistic 3D measurements [61, 62]. Most of these works made use of the classical Cassie-  
42 Baxter (CB) model or some variation of it, assuming thus that the liquid-air interface was a  
43 straight line. Usually, this held true because of the typically small distance between neighboring  
44 surface irregularities.

45  
46  
47  
48  
49  
50  
51  
52  
53  
54  
55  
56  
57  
58  
59  
60  
61  
62  
63  
64  
65  
66  
67  
68  
69  
70  
71  
72  
73  
74  
75  
76  
77  
78  
79  
80  
81  
82  
83  
84  
85  
86  
87  
88  
89  
90  
91  
92  
93  
94  
95  
96  
97  
98  
99  
100  
101  
102  
103  
104  
105  
106  
107  
108  
109  
110  
111  
112  
113  
114  
115  
116  
117  
118  
119  
120  
121  
122  
123  
124  
125  
126  
127  
128  
129  
130  
131  
132  
133  
134  
135  
136  
137  
138  
139  
140  
141  
142  
143  
144  
145  
146  
147  
148  
149  
150  
151  
152  
153  
154  
155  
156  
157  
158  
159  
160  
161  
162  
163  
164  
165  
166  
167  
168  
169  
170  
171  
172  
173  
174  
175  
176  
177  
178  
179  
180  
181  
182  
183  
184  
185  
186  
187  
188  
189  
190  
191  
192  
193  
194  
195  
196  
197  
198  
199  
200  
201  
202  
203  
204  
205  
206  
207  
208  
209  
210  
211  
212  
213  
214  
215  
216  
217  
218  
219  
220  
221  
222  
223  
224  
225  
226  
227  
228  
229  
230  
231  
232  
233  
234  
235  
236  
237  
238  
239  
240  
241  
242  
243  
244  
245  
246  
247  
248  
249  
250  
251  
252  
253  
254  
255  
256  
257  
258  
259  
260  
261  
262  
263  
264  
265  
266  
267  
268  
269  
270  
271  
272  
273  
274  
275  
276  
277  
278  
279  
280  
281  
282  
283  
284  
285  
286  
287  
288  
289  
290  
291  
292  
293  
294  
295  
296  
297  
298  
299  
300  
301  
302  
303  
304  
305  
306  
307  
308  
309  
310  
311  
312  
313  
314  
315  
316  
317  
318  
319  
320  
321  
322  
323  
324  
325  
326  
327  
328  
329  
330  
331  
332  
333  
334  
335  
336  
337  
338  
339  
340  
341  
342  
343  
344  
345  
346  
347  
348  
349  
350  
351  
352  
353  
354  
355  
356  
357  
358  
359  
360  
361  
362  
363  
364  
365  
366  
367  
368  
369  
370  
371  
372  
373  
374  
375  
376  
377  
378  
379  
380  
381  
382  
383  
384  
385  
386  
387  
388  
389  
390  
391  
392  
393  
394  
395  
396  
397  
398  
399  
400  
401  
402  
403  
404  
405  
406  
407  
408  
409  
410  
411  
412  
413  
414  
415  
416  
417  
418  
419  
420  
421  
422  
423  
424  
425  
426  
427  
428  
429  
430  
431  
432  
433  
434  
435  
436  
437  
438  
439  
440  
441  
442  
443  
444  
445  
446  
447  
448  
449  
450  
451  
452  
453  
454  
455  
456  
457  
458  
459  
460  
461  
462  
463  
464  
465  
466  
467  
468  
469  
470  
471  
472  
473  
474  
475  
476  
477  
478  
479  
480  
481  
482  
483  
484  
485  
486  
487  
488  
489  
490  
491  
492  
493  
494  
495  
496  
497  
498  
499  
500  
501  
502  
503  
504  
505  
506  
507  
508  
509  
510  
511  
512  
513  
514  
515  
516  
517  
518  
519  
520  
521  
522  
523  
524  
525  
526  
527  
528  
529  
530  
531  
532  
533  
534  
535  
536  
537  
538  
539  
540  
541  
542  
543  
544  
545  
546  
547  
548  
549  
550  
551  
552  
553  
554  
555  
556  
557  
558  
559  
560  
561  
562  
563  
564  
565  
566  
567  
568  
569  
570  
571  
572  
573  
574  
575  
576  
577  
578  
579  
580  
581  
582  
583  
584  
585  
586  
587  
588  
589  
590  
591  
592  
593  
594  
595  
596  
597  
598  
599  
600  
601  
602  
603  
604  
605  
606  
607  
608  
609  
610  
611  
612  
613  
614  
615  
616  
617  
618  
619  
620  
621  
622  
623  
624  
625  
626  
627  
628  
629  
630  
631  
632  
633  
634  
635  
636  
637  
638  
639  
640  
641  
642  
643  
644  
645  
646  
647  
648  
649  
650  
651  
652  
653  
654  
655  
656  
657  
658  
659  
660  
661  
662  
663  
664  
665  
666  
667  
668  
669  
670  
671  
672  
673  
674  
675  
676  
677  
678  
679  
680  
681  
682  
683  
684  
685  
686  
687  
688  
689  
690  
691  
692  
693  
694  
695  
696  
697  
698  
699  
700  
701  
702  
703  
704  
705  
706  
707  
708  
709  
710  
711  
712  
713  
714  
715  
716  
717  
718  
719  
720  
721  
722  
723  
724  
725  
726  
727  
728  
729  
730  
731  
732  
733  
734  
735  
736  
737  
738  
739  
740  
741  
742  
743  
744  
745  
746  
747  
748  
749  
750  
751  
752  
753  
754  
755  
756  
757  
758  
759  
760  
761  
762  
763  
764  
765  
766  
767  
768  
769  
770  
771  
772  
773  
774  
775  
776  
777  
778  
779  
780  
781  
782  
783  
784  
785  
786  
787  
788  
789  
790  
791  
792  
793  
794  
795  
796  
797  
798  
799  
800  
801  
802  
803  
804  
805  
806  
807  
808  
809  
810  
811  
812  
813  
814  
815  
816  
817  
818  
819  
820  
821  
822  
823  
824  
825  
826  
827  
828  
829  
830  
831  
832  
833  
834  
835  
836  
837  
838  
839  
840  
841  
842  
843  
844  
845  
846  
847  
848  
849  
850  
851  
852  
853  
854  
855  
856  
857  
858  
859  
860  
861  
862  
863  
864  
865  
866  
867  
868  
869  
870  
871  
872  
873  
874  
875  
876  
877  
878  
879  
880  
881  
882  
883  
884  
885  
886  
887  
888  
889  
890  
891  
892  
893  
894  
895  
896  
897  
898  
899  
900  
901  
902  
903  
904  
905  
906  
907  
908  
909  
910  
911  
912  
913  
914  
915  
916  
917  
918  
919  
920  
921  
922  
923  
924  
925  
926  
927  
928  
929  
930  
931  
932  
933  
934  
935  
936  
937  
938  
939  
940  
941  
942  
943  
944  
945  
946  
947  
948  
949  
950  
951  
952  
953  
954  
955  
956  
957  
958  
959  
960  
961  
962  
963  
964  
965  
966  
967  
968  
969  
970  
971  
972  
973  
974  
975  
976  
977  
978  
979  
980  
981  
982  
983  
984  
985  
986  
987  
988  
989  
990  
991  
992  
993  
994  
995  
996  
997  
998  
999  
1000

Complementing seminal works trying to address this issue [63-66], in our recent study [67], we revoked this constraint by deriving the formalism of a refined CB model which, nonetheless, considered curved liquid-air interfaces on various single- and two-level

1  
2  
3 topographies. Direct comparison between our model and the original CB model revealed that  
4 the latter overpredicted substantially the contact angle, while it failed to capture the anticipated  
5 trends between contact angle and roughness. Because of this deviating behavior, the original  
6 CB model did not capture the transitions from the CB state to the Wenzel and Young states  
7 with decreasing surface roughness.  
8  
9  
10  
11  
12  
13  
14

## 15 **2. Materials and Methods**

16  
17 Throughout this work, the basis of the calculations was our refined CB model derived and  
18 applied for the predictions of surface topographies exhibiting superomniphobic traits [67]. The  
19 heart of our methodology lay in the consideration of realistic curved liquid-air interfaces  
20 separating trapped air from supernatant liquid. The radius of the curved meniscus was defined  
21 with the help of the capillary length  $l_{\text{cap}} = \sqrt{\gamma_{\text{la}} / \rho g}$ , which was, in turn, a function of the liquid  
22 surface tension  $\gamma_{\text{la}}$ , the liquid density  $\rho$  and the gravitational acceleration  $g$ . The curvature of  
23 the liquid-air interface was then quantified by considering the sagging (or protrusion) height  $h$   
24  $= l/l_{\text{cap}}$ , where  $l$  was a characteristic topography-dependent length. For all considered single-  
25 level surface topographies,  $l$  was defined accordingly [67].  
26  
27  
28  
29  
30  
31  
32  
33

34 By observing the original CB model,  $\theta^{\text{CB}} = f_{\text{sl}} \cos\theta^{\text{Y}} - f_{\text{la}}$ , where  $f_{\text{sl}}$  and  $f_{\text{la}}$  describe the area  
35 fractions of the solid-liquid and liquid-air interfaces, respectively, and the superscript Y  
36 denotes the contact angle by virtue of Young's relation [52], it becomes obvious that the  
37 calculation of  $\theta^{\text{CB}}$  depends on  $f_{\text{sl}}$  and  $f_{\text{la}}$ , which, in turn, depend on the surface topography type  
38 and the shape of the liquid-air interface. Correspondingly, in our previous work [67], analytical  
39 expressions for  $f_{\text{sl}}$  and  $f_{\text{la}}$  were derived for the 2D pillars, fiber and sinusoidal surface  
40 topographies illustrated in figures 1a, 1b and 1c, respectively. In addition, a generic algebraic  
41 expression for modeling multilevel hierarchical roughness of arbitrarily large multiplicity was  
42 derived based on information on single-level roughness. This expression was employed here  
43 to predict the water contact angle on hierarchical two- and three-level topographies.  
44  
45  
46  
47  
48  
49  
50  
51

52 Our model requires as input physicochemical parameters of the wetting liquid (density  $\rho$  and  
53 surface tension  $\gamma_{\text{la}}$ ), Young contact angle  $\theta^{\text{Y}}$  of the wetting liquid on a completely flat and  
54 smooth surface made of the same material as the rough surface, as well as type and  
55 dimensionality of surface topography. The Young contact angle can be measured  
56 experimentally, or, alternatively, it can be computed by virtue of the Young equation  $\cos\theta^{\text{Y}} =$   
57  
58  
59  
60

$(\gamma_s - \gamma_{sl})/\gamma_{la}$ , where  $\gamma_s$  and  $\gamma_{la}$  are the solid surface energy and liquid surface tension terms, respectively, which can be measured experimentally or be found in material databases. The remaining interfacial surface energy term  $\gamma_{sl}$  cannot be measured directly and thus needs to be computed by using any of the conventional Fowkes [68], Zisman [69] or Owens-Wendt [70] theoretical approximations, with the latter being slightly preferential over the others. Should this be the case, information on the polar and dispersive components of  $\gamma_{la}$  and  $\gamma_s$  is required. Here, the Young contact angle was measured experimentally or, where applicable, was found in the literature (see below) and thus there was no need to resort to measuring the polar and dispersive parts of  $\gamma_{la}$  and  $\gamma_s$ .

The objective of the current work was twofold: on one side, we extended the formalism of our refined CB model from semi-infinite 2D to 3D topographies, whereas, on the other side, we tested and validated our model, in its entirety, by comparing directly model predictions with experimental data for various combinations of surface topographies, hierarchy levels and surface materials. Accordingly, area fractions  $f_{sl}$  and  $f_{la}$  were derived for a new 3D surface topography featuring 3D pillars with square cross section. A schematic illustration of this new single-level topography, along with its characteristic geometric details are shown in figure 1(d). The resulting area fraction relations for this topography are as follows (see supplementary material for derivation):

$$f_{sl} = \frac{W^2}{D_p^2} \quad (1)$$

$$f_{la} = \frac{2l_{arc}W + (l_{arc})^2}{D_p^2} \quad (2)$$

where  $W$  and  $D_p$  represent the width and unit cell distance (see figure 1(d)) and  $l_{arc}$  is the numerator of the corresponding  $f_{la}$  relation for 2D pillars as it was derived in our recent work for different wetting cases, i.e., wetting liquid touches (wets) the surface base level or not [67]. To validate our model, totally eleven single-level surface topographies of various dimensions and types were considered in full compliance with the three basic surface topographies introduced originally [67], namely 2D flat-top pillars (figure 1(a)), fibers with circular cross-section (figure 1(b)) and sinusoids (figure 1(c)). To further validate the ability of our model to capture accurately wetting of surfaces with 3D texture, additionally eight 3D-pillar topographies of various dimensions were used for a total of nineteen single-level surface topographies (2D and 3D). Figures 1(e)-(h) describe representative experimental surfaces

1  
2  
3 displaying 2D-pillar, sinusoidal and 3D-pillar topography, respectively. Furthermore, to  
4 validate our model predictions related to multilevel topography, twelve two-level and one  
5 three-level hierarchical surfaces were studied. Representative 2D schematic illustrations of the  
6 two- and three-level surface topographies considered here are shown in Figure 2. Accordingly,  
7 figure 2a illustrates the “pillars on sinusoids” topography corresponding to structures 20-22 in  
8 Table 2, figure 2b shows the “sinusoids on sinusoids” topography describing structures 23-31  
9 in Table 2, whereas figure 2c displays the “triple sinusoidal” topography of structure 32 in  
10 Table 2. A detailed description of the characteristic geometrical parameters of the experimental  
11 single- and multilevel surface topographies considered here is provided in Tables 1 and 2,  
12 respectively. Given the great technological importance of surfaces exhibiting patterns of  
13 diverse length scales, caution was taken here that a broad spectrum of characteristic lengths  
14 was spanned ranging from a few hundreds of micrometers to a few tens of nanometers (cf.  
15 Tables 1 and 2). This corroborates the generic validity and applicability of our model.

16  
17 Throughout this work, the wetting liquid was water having density  $\rho$  and surface tension  $\gamma_{la}$  at  
18 ambient conditions equal to  $997 \text{ kg/m}^3$  and  $72.8 \text{ mN/m}$ , respectively. To extract conclusions  
19 on the generic character of our model, a rich variety of surface materials was considered  
20 involving silanized silicon wafers, poly(lactic-*co*-glycolic) acid (PLGA) comprising 85%  
21 polylactic acid (PLA) and 15% polyglycolic acid (PGA), cyclic olefin copolymer (COC),  
22 polydimethylsiloxane (PDMS), aluminium and an epoxy-based shape memory polymer  
23 (SMP). Structures 1-3 in Table 1 were fabricated on silicon wafers using standard UV-  
24 lithographic techniques. Briefly, silicon wafers were spin-coated with a positive photoresist  
25 and exposed to UV light in an EVG 620 mask aligner using a designed chromium-on-glass  
26 photomask. After photoresist development, a Deep Reactive Ion Etching (DRIE) process was  
27 carried out in an Oxford Plasmalab 80+ machine to etch the silicon in the areas not covered by  
28 the photoresist. After etching, the remaining photoresist was removed by successive sonication  
29 in acetone, IPA and deionized water.

30  
31 Then, the wafer was fluorinated by exposure for 30 min to a saturated atmosphere of vapor  
32 PFOCTS. Structures 9-11 were fabricated using a picosecond laser Nd:YVO<sub>4</sub> (3D MicroMac  
33 Microstruct) with pulses of 10 ps and wavelength of 1064, 532 and 355 nm, respectively.  
34 Therein, the beam diameter was smaller than  $30 \mu\text{m}$ . Contact angle measurements for structures  
35 1-3 and 9-11 were performed on a Surftens Universal (OEG) goniometer. Analogously,  
36 polymer-based surface topographies 4 and 12-14 were fabricated by hot embossing on a  
37 Jenoptik HEX 03 using a silicon wafer with test patterns manufactured by photolithography  
38 and subsequent etching. Hot embossing was carried out at  $100 \text{ }^\circ\text{C}$  for PLGA and at  $120 \text{ }^\circ\text{C}$  for  
39  
40  
41  
42  
43  
44  
45  
46  
47  
48  
49  
50  
51  
52  
53  
54  
55  
56  
57  
58  
59  
60

1  
2  
3 COC. Water contact angle measurements were performed on a Krüss drop shape analyzer  
4 (DSA 100).. For all surfaces constructed in the context of this work (cf. Table 1), the Young  
5 contact angle of water was measured with the help of the goniometers reported above.  
6  
7  
8  
9  
10  
11  
12  
13  
14  
15  
16  
17  
18  
19  
20  
21  
22  
23  
24  
25  
26  
27  
28  
29  
30  
31  
32  
33  
34  
35  
36  
37  
38  
39  
40  
41  
42  
43  
44  
45  
46  
47  
48  
49  
50  
51  
52  
53  
54  
55  
56  
57  
58  
59  
60



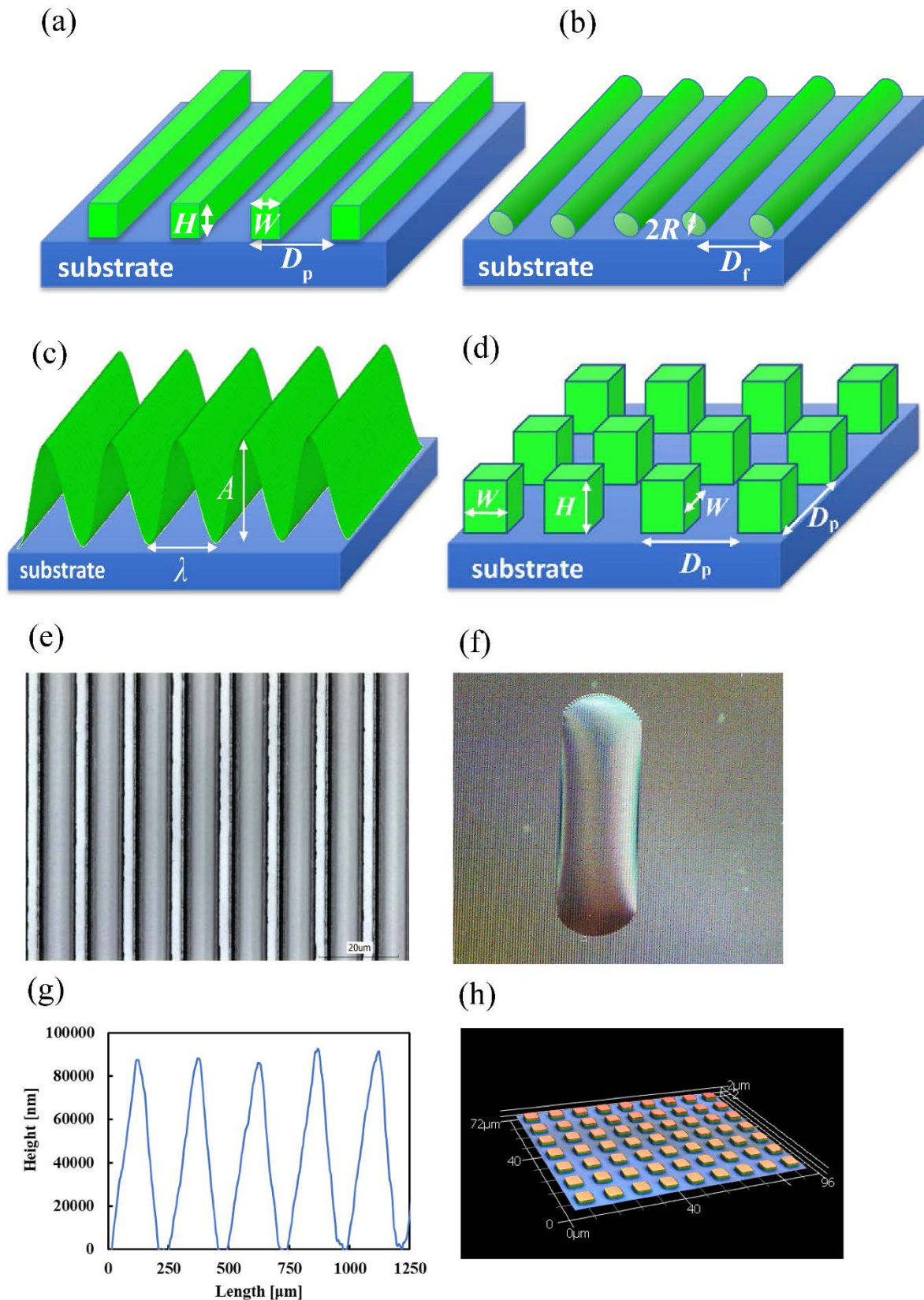
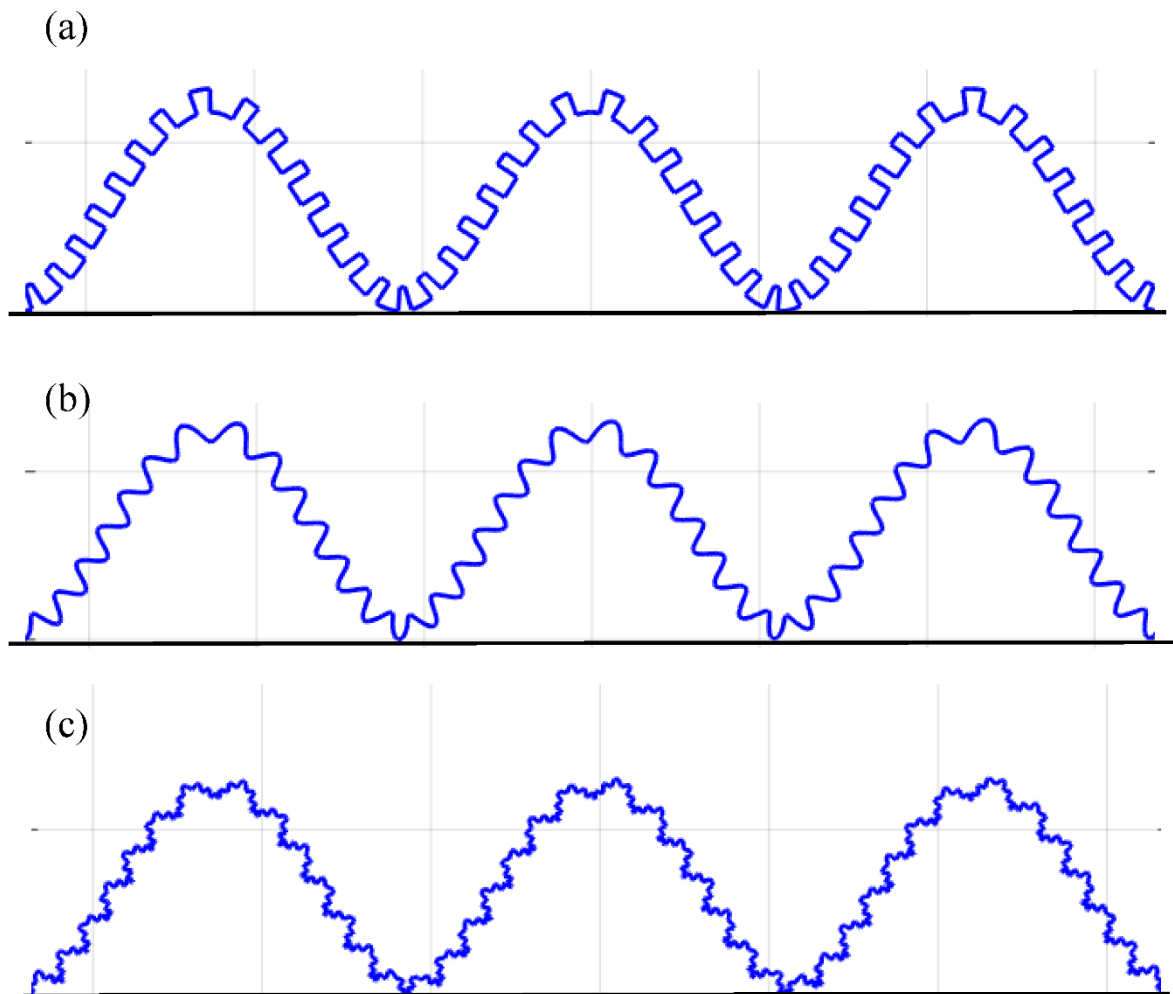


**Figure 1.** Schematic illustration of single-level (a) 2D-pillar, (b) fiber, (c) sinusoidal and (d) 3D-pillar topographies. Relevant geometric parameters are also shown. (e) Confocal laser scanning microscopy (CLSM) top view of a representative 2D-pillar topography corresponding

1  
2  
3 to structure 4 in table 1, (f) pronounced anisotropic wetting by water (picture taken from  
4 underneath the wetted sample of part (e), (g) Profile of an indicative sinusoidal topography  
5 corresponding to structure 9 in table 1 measured by a mechanical profilometer (Veeco Dektrak-  
6 8 with 0.7  $\mu\text{m}$  tip) and (h) CSLM 3D view of a representative 3D-pillar topography  
7 corresponding to structure 13 in table 1.  
8  
9  
10  
11  
12  
13  
14



46 **Figure 2.** Representative 2D schematic illustrations of the hierarchical two-level a) pillars on  
47 sinusoids, b) sinusoids on sinusoids and c) three-level triple sinusoidal surface topographies  
48 described in Table 2.  
49  
50  
51  
52  
53  
54

55 **Table 1.** Description of single-level surface topographies considered here. Symbols  $H$ ,  $W$  and  
56  $D_p$  correspond to pillar height, width and unit cell distance, respectively, whereas  $R$  and  $D_f$   
57 describe the fiber radius and unit cell distance, respectively. Finally,  $A$  and  $\lambda$  represent the  
58  
59  
60

amplitude and wavelength of the sinusoidal topography, respectively. Experimental Young's contact angle  $\theta^Y$  of water on each surface is also reported.

Structure #	Topography	Dimensions [ $\mu\text{m}$ ]	Surface material	$\theta^Y$ [ $^\circ$ ]	Ref.
1	2D Pillars	$H = 0.253, W = 25, D_p = 50$	silanized silicon wafer	116.7	this work
2	2D Pillars	$H = 0.253, W = 50, D_p = 100$	silanized silicon wafer	116.7	this work
3	2D Pillars	$H = 0.253, W = 100, D_p = 200$	silanized silicon wafer	116.7	this work
4	2D Pillars	$H = 4.4, W = 3.4, D_p = 12$	PLGA	72.7	this work & [71]
5	2D Pillars	$H = 10, W = 45.5, D_p = 90.6$	COC	88.3	[72]
6	fibers	$R = 18, D_f = 79$	PDMS	105	[8]
7	fibers	$R = 12.5, D_f = 63$	PDMS	105	[8]
8	fibers	$R = 14, D_f = 78$	PDMS	105	[8]
9	sinusoidal	$A = 86, \lambda = 225$	aluminium	67.1	this work
10	sinusoidal	$A = 96, \lambda = 280$	aluminium	67.1	this work
11	sinusoidal	$A = 90, \lambda = 480$	aluminium	67.1	this work
12	3D Pillars	$H = 1.6, W = 2.6, D_p = 3.9$	COC	93	this work
13	3D Pillars	$H = 1.7, W = 6.0, D_p = 10.4$	COC	93	this work
14	3D Pillars	$H = 1.8, W = 3.9, D_p = 6.6$	COC	93	this work
15	3D Pillars	$H = 8.6, W = 44.7, D_p = 90.6$	COC	88.3	[72]
16	3D Pillars	$H = 8.0, W = 45.5, D_p = 90.6$	COC	88.3	[72]
17	3D Pillars	$H = 10.0, W = 10.0, D_p = 20.0$	SMP	89	[73]

18	3D Pillars	$H = 10.0, W = 10.0, D_p = 30.0$	SMP	89	[73]
19	3D Pillars	$H = 10.0, W = 10.0, D_p = 40.0$	SMP	89	[73]

**Table 2.** Description of hierarchical multilevel surface topographies considered here. Symbols are identical to Table 1. Subscripts 1, 2 and 3 (where applicable) denote different levels starting from the finest towards coarser ones. Experimental Young's contact angle  $\theta^Y$  of water on each surface is also reported.

Structure #	Topography	Dimensions [ $\mu\text{m}$ ]	Surface material	$\theta^Y$ [ $^\circ$ ]	Ref.
20	pillars on sinusoids	$H = 0.15, W = 0.3, D_p = 0.5$ $A = 4.4, \lambda = 31$	PDMS	110	[74]
21	pillars on sinusoids	$H = 0.35, W = 0.2, D_p = 0.5$ $A = 4.4, \lambda = 31$	PDMS	110	[74]
22	pillars on sinusoids	$H = 0.7, W = 0.15, D_p = 0.5$ $A = 4.4, \lambda = 31$	PDMS	110	[74]
23	sinusoids on sinusoids	$A_1 = 0.275, \lambda_1 = 0.822$ $A_2 = 0.6, \lambda_2 = 25$	PDMS	119	[75]
24	sinusoids on sinusoids	$A_1 = 0.322, \lambda_1 = 0.774$ $A_2 = 2.75, \lambda_2 = 39$	PDMS	119	[75]
25	sinusoids on sinusoids	$A_1 = 0.305, \lambda_1 = 0.79$ $A_2 = 3.5, \lambda_2 = 39$	PDMS	119	[75]
26	sinusoids on sinusoids	$A_1 = 0.311, \lambda_1 = 0.825$ $A_2 = 4.35, \lambda_2 = 34$	PDMS	119	[75]
27	sinusoids on sinusoids	$A_1 = 0.247, \lambda_1 = 0.77$ $A_2 = 2.5, \lambda_2 = 16.7$	PDMS	119	[75]
28	sinusoids on sinusoids	$A_1 = 0.297, \lambda_1 = 0.8$ $A_2 = 4.5, \lambda_2 = 25.8$	PDMS	119	[75]
29	sinusoids on sinusoids	$A_1 = 0.27, \lambda_1 = 0.776$ $A_2 = 3.75, \lambda_2 = 20$	PDMS	119	[75]
30	sinusoids on sinusoids	$A_1 = 0.315, \lambda_1 = 0.815$ $A_2 = 4.5, \lambda_2 = 23.3$	PDMS	119	[75]
31	sinusoids on sinusoids	$A_1 = 0.267, \lambda_1 = 0.75$ $A_2 = 4.2, \lambda_2 = 21.4$	PDMS	119	[75]
32	triple sinusoidal	$A_1 = 0.075, \lambda_1 = 0.15$ $A_2 = 0.45, \lambda_2 = 0.9$ $A_3 = 5, \lambda_3 = 10$	PDMS	110	[76]

### 3. Results and Discussion

#### 3.1 Single-level topographies

Figures 3 and 4 illustrate comparisons between calculated contact angles and their experimental counterparts for the nineteen single-level surface topographies listed in Table 1. In particular, figure 3 shows contact angle comparisons for 2D pillars, fibers, and sinusoidal topographies, whereas figure 4 for 3D pillars. For the 2D pillars case, depicted in figure 3, the agreement between experiment and model was gratifying resulting to an average error of about 6%. This was, at least partially, attributed to the inherent assumption of our model pertaining to pinning of the liquid at the corners of the pillars. This assumption hampered the droplet from intruding in the free space between neighboring pillars thus causing artificially increased contact angles as evinced by figure 3. Nonetheless, this discrepancy lay for three of the totally five tested structures displaying this topography within the uncertainties of the experimental data. The model results for the fiber topography, shown in figure 3, were substantially closer to their experimental counterparts giving rise to an average error below 3%. Clearly, figure 3 shows that the attained contact angles for the fiber topography were larger than the ones for 2D pillars, thereby corroborating previous modeling observations and associated trends [67] relating this behavior with the re-entrant geometry of the fiber topography.

The calculated contact angles for the sinusoidal topography were substantially smaller than the previous two single-level topographies, namely 2D pillars and fibers. This observation becomes apparent by juxtaposing the three topographies shown in figure 3 and is in excellent agreement with recent theoretical predictions identifying fibers as the most efficacious amongst the three single-level topographies for achieving high contact angles, followed, in order of efficiency, by 2D pillars and finally sinusoidal surfaces [67]. Figure 3 shows that the agreement between experimental measurements and model predictions for sinusoidal topographies was remarkably good exhibiting an average error of only 4.6%.

Next, consideration of actual 3D surface topographies, instead of simplified semi-infinite 2D structures, resulted in increased water contact angles and thus enhanced water repellency. This behavior is illustrated in figure 4 for the 3D-pillars case and was attributed to an augmented surface-to-volume ratio, generally more pronounced in 3D structures than in commensurate 2D topographies, inducing thereby increased surface roughness and thus enhanced liquid-repellency. The predicted contact angles were, once again, in reasonable accord with experimental observations displaying average deviations of not more than 4.5%. Taken all together, predicted contact angles for the four types of single-level topographies considered

here (see Table 1) deviated, on average, from experimental measurements by less than 5%. This discrepancy was, for most surface topographies examined here, within the statistical uncertainties of experimental data.

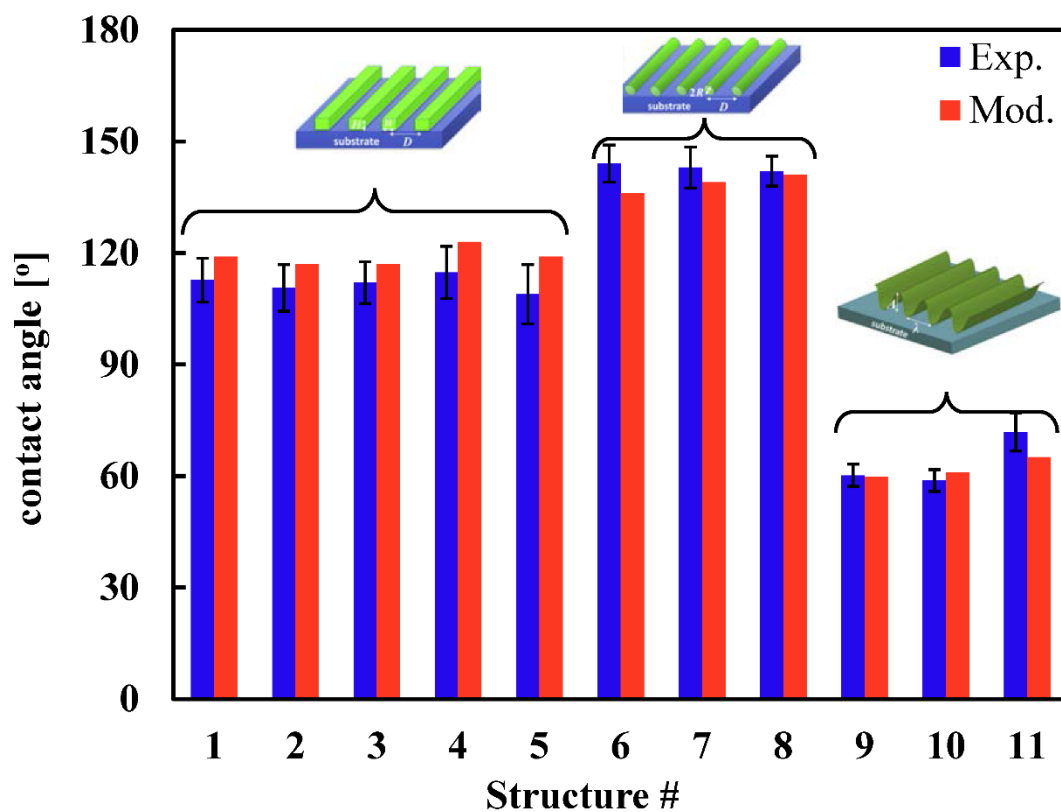


**Figure 3.** Contact angle comparison between model results (red) and experimental data (blue) for eleven single-level topographies: structures 1-5, 6-8 and 9-11 correspond to 2D pillars, fibers and sinusoid topographies, respectively (see Table 1 and Ref. [67]).

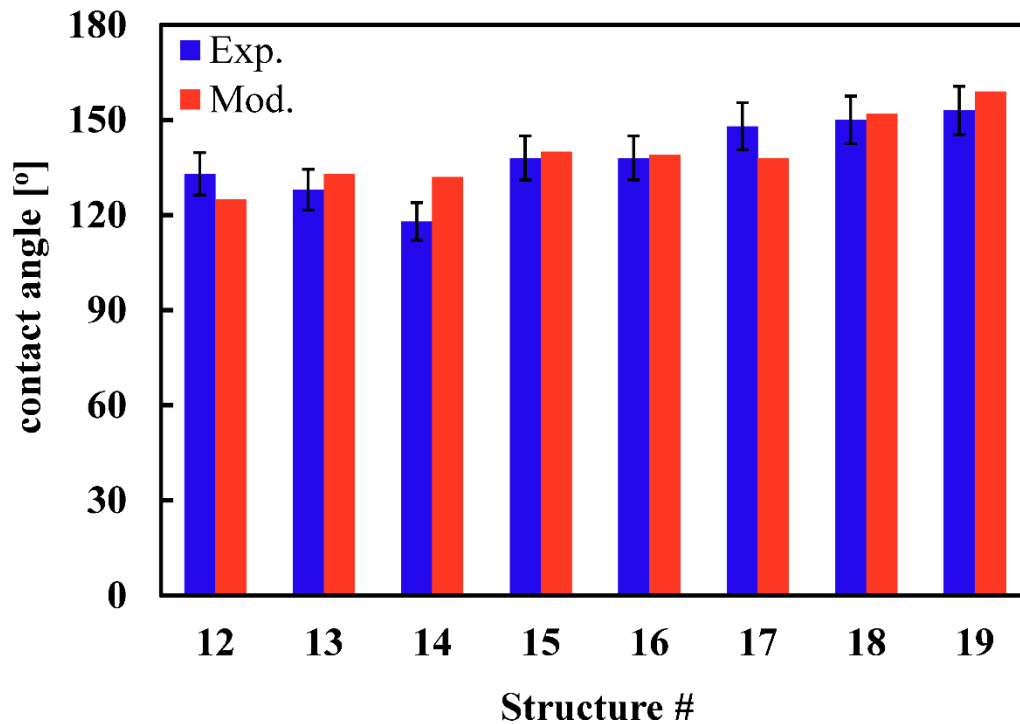


**Figure 4.** Contact angle comparison between model results (red) and experimental data (blue) for eight single-level topographies with 3D-pillars texture (see Table 1 and figure 1).

### 3.2 Multilevel topographies

It is well established in the literature that multilevel hierarchical surface topographies induced enhanced liquid repellency. Figure 5 validates this consensus by illustrating calculated and experimentally measured contact angles for two types of two-level topography. For most structures in figure 5, contact angles lay in the vicinity of  $140^\circ$ , with two surfaces exhibiting superhydrophobic behavior ( $\theta > 150^\circ$ ). Structures 20-22 in figure 5 correspond to two-level topographies featuring pillars (fine level) on top of sinusoids (coarse level), wherein the two levels differed in size by at least one order of magnitude (see table 2). This observation validates previous theoretical findings arguing that a size difference of at least one order of magnitude between the superimposed surface patterns was required for achieving superhydrophobicity [67]. Notwithstanding the significance and influence of multilevel hierarchical structures on liquid repellency, the construction of such surfaces poses substantial technological challenges. This is due to the intrinsic technological difficulties associated with manufacturing of surface details on the submicron or even nanoscale.

Structures 23-31 in figure 5 correspond to “sinusoids on sinusoids” two-level topographies giving rise to contact angles consistently smaller than the ones for “pillars on sinusoids”

1  
2  
3 surfaces. Given that the surface material was in both cases the same (PDMS), the coarse level  
4 was of the same type (sinusoids) and, more or less, on the same order of magnitude (table 2),  
5 we discerned that the behavior of two-level topographies was greatly influenced by the upper  
6 (finer) level. According to the single-level results reported in Section 3.1, 2D-pillar surfaces  
7 exhibited, in general, larger contact angles than sinusoidal topographies. The behavior shown  
8 in figure 5 is, therefore, consistent with this observation. For both types of two-level  
9 topography considered here, the calculated contact angles were in notable accord with their  
10 experimental counterparts. The average deviation for the “pillars on sinusoids” and “sinusoids  
11 on sinusoids” topographies amounted to 4.7% and 3.2%, respectively, resulting in an average  
12 deviation of 4% for the two-level topographies.

13  
14  
15  
16  
17  
18  
19  
20 Finally, figure 6 shows the comparison between the predicted and the experimental contact  
21 angle for a three-level topography with three levels of sinusoid, each having dimensions that  
22 differed by one order of magnitude from the next one (table 2). Superhydrophobicity was  
23 observed here as well, further validating the general belief that multilevel topographies enable  
24 increased liquid-repellency. Indeed, this becomes clear by comparing the contact angles for  
25 sinusoidal single-, two- and three-level topographies shown in figures 3 (structures 9-11), 4  
26 (structures 23-31) and 5, respectively. The addition of a second level of sinusoidal patterns  
27 almost doubled the observed contact angle, while incorporation of a third sinusoidal level  
28 brought about an additional 12.5% contact angle increase. Again, our model predicted for this  
29 three-level surface topography a contact angle that deviated only by 3.1% from the  
30 experimentally measured value, well within the statistical uncertainty of the experimental  
31 measurement. Taken all together, figures 5, 6 and the discussion therein confirmed the ability  
32 of our model to predict very accurately the wetting behavior of surfaces exhibiting multilevel  
33 hierarchical topographies.  
34  
35  
36  
37  
38  
39  
40  
41  
42  
43  
44  
45  
46  
47  
48  
49  
50  
51  
52  
53  
54  
55  
56  
57  
58  
59  
60



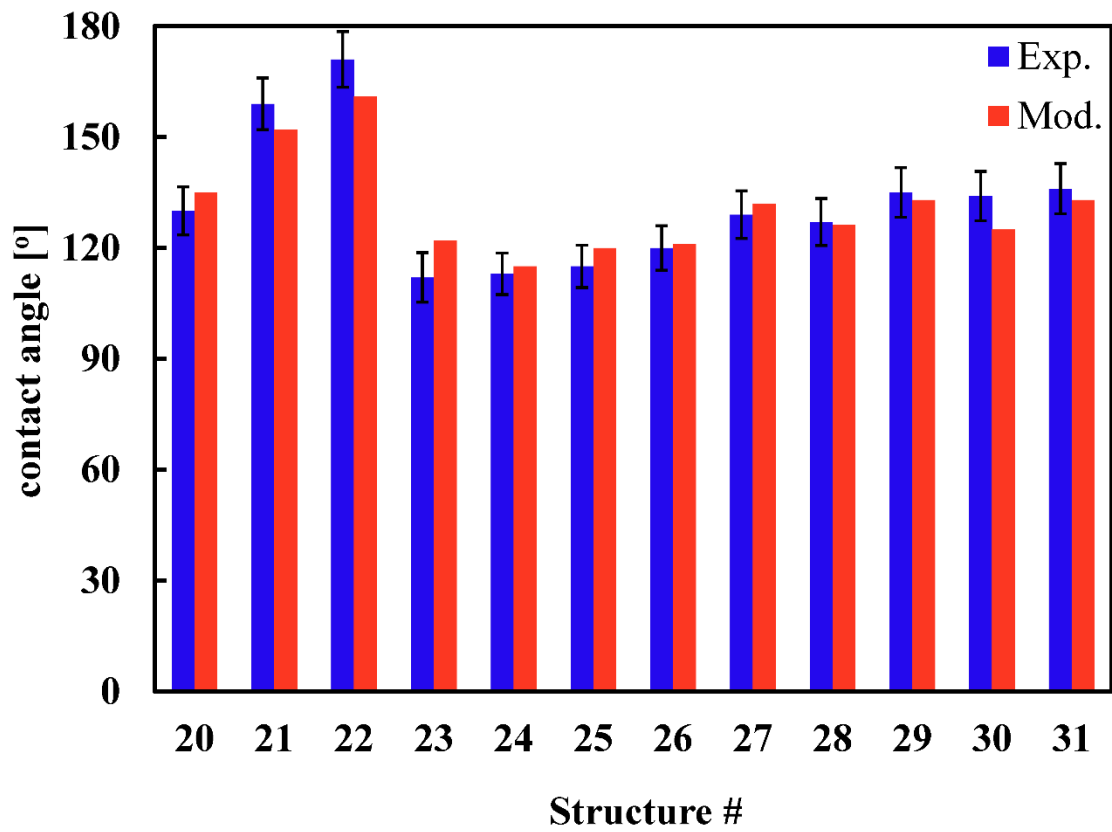


**Figure 5.** Contact angle comparison between model results (red) and experimental data (blue) for twelve two-level surface topographies: Structures 20-22 describe “pillars on sinusoids”, whereas structures 23-31 correspond to “sinusoids on sinusoids” topographies. (see Table 2).

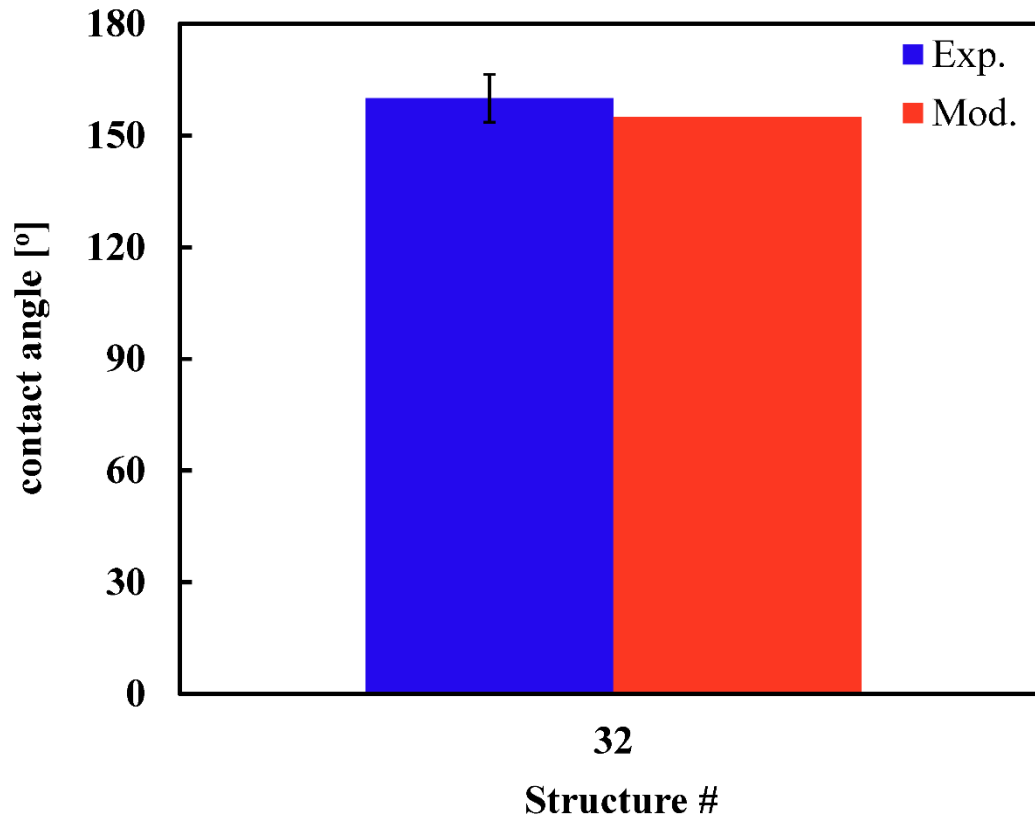


**Figure 6.** Contact angle comparison between model results (red) and experimental data (blue) for a three-level surface topography corresponding to three levels of sinusoids placed on top of each other (see Table 2).

#### 4. Conclusions

The objective of this work is twofold; on one side, we report the extension of the formalism of our recently published wetting model [67] to account for 3D pillar topographies, while, on the other hand, we provide compelling evidence on the validation of our model in capturing accurately the wetting behavior across various topography types, surface materials and hierarchy levels. Realistic engineered surfaces featuring single-, two- and three-level surface topographies, found either in the literature or fabricated and analyzed in the context of this work, were utilized for validation purposes. One-to-one comparison between modeling results and experimental data validated our original theoretical hypothesis that, in general, multilevel hierarchical topographies enable enhanced liquid-repellency, constituting thereby a valuable tool for achieving superhydrophobicity.

1  
2  
3 Of the four single-level surface topographies considered here, the 3D pillars exhibited the  
4 highest contact angles, in some cases exceeding  $150^\circ$ , owed to increased surface-to-volume  
5 ratio compared to the commensurate semi-infinite 2D textures. Subsequently, the fiber  
6 topography, presenting re-entrant geometry, yielded the largest contact angles among the single  
7 level 2D topographies, followed by the 2D pillars and sinusoidal topographies. Increased water  
8 repellency was, in general, observed for two-level hierarchical surfaces, while three-level  
9 sinusoidal hierarchical surfaces yielded contact angles as high as  $165^\circ$ . For the three-level  
10 sinusoidal topography, addition of a second level of sinusoidal patterns almost doubled the  
11 observed contact angle, while incorporation of a third sinusoidal level brought about an  
12 additional 12.5% contact angle increase. In all cases of multilevel topographies considered  
13 here, the different superposing levels had length scales differing in size from one another by at  
14 least one order of magnitude.

15  
16  
17 Our model predictions were for all single-level topographies considered here in gratifying  
18 agreement with experimental contact angle measurements resulting to an average error of  
19 4.6%, well within the experimental statistical uncertainty. Analogous comparisons for two- and  
20 three-level topographies resulted in average deviations of about 3.5%. Taken all together, our  
21 refined wetting model captured remarkably well and within experimental inaccuracies the  
22 wetting behavior of water on various materials exhibiting single- and multilevel hierarchical  
23 roughness. Modelling wettability accurately across different wetting liquids, surface materials  
24 and topographies sets the foundations of a generic surface design methodology enabling  
25 tailored wetting properties for numerous technological applications relevant to packaging,  
26 circular economy of materials, waste reduction, recycling, as well as conservation of energy  
27 and natural resources.

## 28 **Acknowledgements**

29  
30 NL and RK gratefully acknowledge the University of Applied Sciences Western Switzerland  
31 (HES-SO), the College of Engineering and Architecture Fribourg (HEIA-FR) and the  
32 MARKETPLACE (Materials Modelling Marketplace for Increased Industrial Innovation)  
33 project funded by the Horizon 2020 EU program under the NMBP-25-2017 call, with Grant  
34 agreement number 760173 (<https://the-marketplace-project.eu/>) for financial support. PMK  
35 gratefully acknowledges the Swiss Nanoscience Institute (SNI) for funding of the projects  
36 PATCELL and REPALL with grant numbers 09.10 and 10.07, respectively, under the  
37  
38  
39  
40  
41  
42  
43  
44  
45  
46  
47  
48  
49  
50  
51  
52  
53  
54  
55  
56  
57  
58  
59  
60

1  
2  
3 framework of the Nanoargovia program. RDA acknowledges funding from the BIOSMART  
4 project belonging to the Bio Based Industries Joint Undertaking under the European Union's  
5 Horizon 2020 - Research and Innovation Framework Program with Grant agreement number  
6 745762. Computational time and resources for this work were granted by the Department of  
7  
8 Computer Science and Communication Systems at HEIA-FR.  
9  
10  
11  
12  
13  
14

### 15 **Data availability statement**

16  
17 The data supporting the findings of this study is available from the corresponding author  
18 upon reasonable request.  
19  
20  
21  
22  
23

### 24 **ORCID iDs**

25  
26 Nikolaos Lempesis: <https://orcid.org/0000-0002-4104-9666>, Ruth Díez-Ahedo  
27 <https://orcid.org/0000-0002-8033-0792>, Per Magnus Kristiansen: [https://orcid.org/0000-0001-](https://orcid.org/0000-0001-7714-0966)  
28 [7714-0966](https://orcid.org/0000-0001-7714-0966)  
29  
30  
31  
32  
33

### 34 **References**

- 35  
36  
37 [1] Adhikari B, Howes T, Bhandari B R and Truong V 2001 STICKINESS IN FOODS: A REVIEW OF  
38 MECHANISMS AND TEST METHODS *International Journal of Food Properties* **4** 1-33  
39 [2] Harte B R, Gray J I and Miltz J 1987 *Food Product-Package Compatibility*: Taylor & Francis)  
40 [3] Michalski M C, Desobry S and Hardy J 1997 Food materials adhesion: a review *Critical reviews*  
41 *in food science and nutrition* **37** 591-619  
42 [4] Criado M, Suárez B and Ferreirós C 1994 The importance of bacterial adhesion in the dairy  
43 industry *Food Technology* **48** 123-6  
44 [5] Nosonovsky M and Bhushan B 2008 Roughness-induced superhydrophobicity: a way to design  
45 non-adhesive surfaces *Journal of Physics: Condensed Matter* **20** 225009  
46 [6] Höcker H 2002 Plasma treatment of textile fibers *Pure and applied chemistry* **74** 423-7  
47 [7] Zimmermann J, Reifler F A, Fortunato G, Gerhardt L-C and Seeger S 2008 A Simple, One-Step  
48 Approach to Durable and Robust Superhydrophobic Textiles *Advanced Functional Materials*  
49 **18** 3662-9  
50 [8] Shabanian S, Khatir B, Nisar A and Golovin K 2020 Rational design of perfluorocarbon-free  
51 oleophobic textiles *Nature Sustainability*  
52 [9] Gao X, Yan X, Yao X, Xu L, Zhang K, Zhang J, Yang B and Jiang L 2007 The Dry-Style Antifogging  
53 Properties of Mosquito Compound Eyes and Artificial Analogues Prepared by Soft Lithography  
54 *Advanced Materials* **19** 2213-7  
55 [10] Cao L, Jones A K, Sikka V K, Wu J and Gao D 2009 Anti-Icing Superhydrophobic Coatings  
56 *Langmuir* **25** 12444-8  
57  
58  
59  
60

- 1  
2  
3 [11] Pan Q and Wang M 2009 Miniature Boats with Striking Loading Capacity Fabricated from  
4 Superhydrophobic Copper Meshes *ACS Applied Materials & Interfaces* **1** 420-3  
5 [12] Ou J, Perot B and Rothstein J P 2004 Laminar drag reduction in microchannels using  
6 ultrahydrophobic surfaces *Physics of Fluids* **16** 4635-43  
7 [13] Marmur A 2006 Underwater Superhydrophobicity: Theoretical Feasibility *Langmuir* **22** 1400-  
8 2  
9 [14] Gurera D and Bhushan B 2019 Optimization of bioinspired conical surfaces for water collection  
10 from fog *Journal of Colloid and Interface Science* **551** 26-38  
11 [15] Wilson S J and Hutley M C 1982 The optical properties of 'moth eye' antireflection surfaces  
12 *Optica Acta: International Journal of Optics* **29** 993-1009  
13 [16] Carlo M and Metin S 2006 A biomimetic climbing robot based on the gecko *Journal of Bionic*  
14 *Engineering* **3** 115-25  
15 [17] Arzt E, Gorb S and Spolenak R 2003 From micro to nano contacts in biological attachment  
16 devices *Proceedings of the National Academy of Sciences* **100** 10603  
17 [18] Solga A, Cerman Z, Striffler B F, Spaeth M and Barthlott W 2007 The dream of staying clean:  
18 Lotus and biomimetic surfaces *Bioinspiration & biomimetics* **2** S126  
19 [19] Dean B and Bhushan B 2010 Shark-skin surfaces for fluid-drag reduction in turbulent flow: a  
20 review *Philosophical Transactions of the Royal Society A: Mathematical, Physical and*  
21 *Engineering Sciences* **368** 4775-806  
22 [20] Bushnell D M and Moore K J 1991 Drag reduction in nature *Annual review of fluid mechanics*  
23 **23** 65-79  
24 [21] Nosonovsky M and Bhushan B 2009 Superhydrophobic surfaces and emerging applications:  
25 Non-adhesion, energy, green engineering *Current Opinion in Colloid & Interface Science* **14**  
26 270-80  
27 [22] Nakajima A, Fujishima A, Hashimoto K and Watanabe T 1999 Preparation of Transparent  
28 Superhydrophobic Boehmite and Silica Films by Sublimation of Aluminum Acetylacetonate  
29 *Advanced Materials* **11** 1365-8  
30 [23] Chen W, Fadeev A Y, Hsieh M C, Öner D, Youngblood J and McCarthy T J 1999  
31 Ultrahydrophobic and Ultralyophobic Surfaces: Some Comments and Examples *Langmuir* **15**  
32 3395-9  
33 [24] Kijlstra J, Reihs K and Klamt A 2002 Roughness and topology of ultra-hydrophobic surfaces  
34 *Colloids and Surfaces A: Physicochemical and Engineering Aspects* **206** 521-9  
35 [25] Herminghaus S 2000 Roughness-induced non-wetting *EPL (Europhysics Letters)* **52** 165  
36 [26] Sun T, Wang G, Feng L, Liu B, Ma Y, Jiang L and Zhu D 2004 Reversible switching between  
37 superhydrophilicity and superhydrophobicity *Angewandte Chemie International Edition* **43**  
38 357-60  
39 [27] Zhang J, Lu X, Huang W and Han Y 2005 Reversible Superhydrophobicity to Superhydrophilicity  
40 Transition by Extending and Unloading an Elastic Polyamide Film *Macromolecular Rapid*  
41 *Communications* **26** 477-80  
42 [28] Lu X, Zhang C and Han Y 2004 Low-Density Polyethylene Superhydrophobic Surface by Control  
43 of Its Crystallization Behavior *Macromolecular Rapid Communications* **25** 1606-10  
44 [29] Seemann R, Brinkmann M, Herminghaus S, Khare K, Law B M, McBride S, Kostourou K,  
45 Gurevich E, Bommer S and Herrmann C 2011 Wetting morphologies and their transitions in  
46 grooved substrates *Journal of Physics: Condensed Matter* **23** 184108  
47 [30] Khare K, Brinkmann M, Law B M, Herminghaus S and Seemann R 2009 Switching wetting  
48 morphologies in triangular grooves *The European Physical Journal Special Topics* **166** 151-4  
49 [31] Nishino T, Meguro M, Nakamae K, Matsushita M and Ueda Y 1999 The Lowest Surface Free  
50 Energy Based on -CF<sub>3</sub> Alignment *Langmuir* **15** 4321-3  
51 [32] Tuteja A, Choi W, Ma M, Mabry J M, Mazzella S A, Rutledge G C, McKinley G H and Cohen R E  
52 2007 Designing superoleophobic surfaces *Science* **318** 1618-22  
53  
54  
55  
56  
57  
58  
59  
60

- 1  
2  
3 [33] Chauhan P, Kumar A and Bhushan B 2019 Self-cleaning, stain-resistant and anti-bacterial  
4 superhydrophobic cotton fabric prepared by simple immersion technique *Journal of Colloid*  
5 *and Interface Science* **535** 66-74  
6 [34] Li F, Bhushan B, Pan Y and Zhao X 2019 Bioinspired superoleophobic/superhydrophilic  
7 functionalized cotton for efficient separation of immiscible oil-water mixtures and oil-water  
8 emulsions *Journal of Colloid and Interface Science* **548** 123-30  
9 [35] Nanda D, Sahoo A, Kumar A and Bhushan B 2019 Facile approach to develop durable and  
10 reusable superhydrophobic/superoleophilic coatings for steel mesh surfaces *Journal of Colloid*  
11 *and Interface Science* **535** 50-7  
12 [36] Gurera D and Bhushan B 2018 Fabrication of bioinspired superliquiphobic synthetic leather  
13 with self-cleaning and low adhesion *Colloids and Surfaces A: Physicochemical and Engineering*  
14 *Aspects* **545** 130-7  
15 [37] Alinezhadfar M, Nasiri Khalil Abad S and Mozammel M 2020 Multifunctional cobalt coating  
16 with exceptional amphiphobic properties: self-cleaning and corrosion inhibition *Surfaces and*  
17 *Interfaces* **21** 100744  
18 [38] Nasiri Khalil Abad S, Najibi Ilkhechi N, Adel M and Mozammel M 2020 Hierarchical architecture  
19 of a superhydrophobic Cd-Si co-doped TiO<sub>2</sub> thin film *Applied Surface Science* **533** 147495  
20 [39] Nasiri Khalil Abad S, Mozammel M, Moghaddam J, Mostafaei A and Chmielus M 2020 Highly  
21 porous, flexible and robust cellulose acetate/Au/ZnO as a hybrid photocatalyst *Applied*  
22 *Surface Science* **526** 146237  
23 [40] Bhushan B and Martin S 2018 Substrate-independent superliquiphobic coatings for water, oil,  
24 and surfactant repellency: An overview *Journal of Colloid and Interface Science* **526** 90-105  
25 [41] Tuteja A, Choi W, Mabry J M, McKinley G H and Cohen R E 2008 Robust omniphobic surfaces  
26 *Proceedings of the National Academy of Sciences* **105** 18200  
27 [42] Cheng Y-T and Rodak D E 2005 Is the lotus leaf superhydrophobic? *Applied Physics Letters* **86**  
28 144101  
29 [43] Marmur A 2003 Wetting on Hydrophobic Rough Surfaces: To Be Heterogeneous or Not To  
30 Be? *Langmuir* **19** 8343-8  
31 [44] Nosonovsky M 2007 Multiscale Roughness and Stability of Superhydrophobic Biomimetic  
32 Interfaces *Langmuir* **23** 3157-61  
33 [45] Bittoun E and Marmur A 2012 The role of multiscale roughness in the lotus effect: is it essential  
34 for super-hydrophobicity? *Langmuir* **28** 13933-42  
35 [46] Nosonovsky M and Bhushan B 2008 Biologically inspired surfaces: broadening the scope of  
36 roughness *Advanced Functional Materials* **18** 843-55  
37 [47] Zhai L, Cebeci F C, Cohen R E and Rubner M F 2004 Stable superhydrophobic coatings from  
38 polyelectrolyte multilayers *Nano letters* **4** 1349-53  
39 [48] Chhatre S S, Choi W and Tuteja A 2010 Scale Dependence of Omniphobic Mesh Surfaces  
40 *Langmuir* **26** 4027-35  
41 [49] Ma M and Hill R M 2006 Superhydrophobic surfaces *Current opinion in colloid & interface*  
42 *science* **11** 193-202  
43 [50] Barbieri L, Wagner E and Hoffmann P 2007 Water wetting transition parameters of  
44 perfluorinated substrates with periodically distributed flat-top microscale obstacles *Langmuir*  
45 **23** 1723-34  
46 [51] Kang S M, You I, Cho W K, Shon H K, Lee T G, Choi I S, Karp J M and Lee H 2010 One-step  
47 modification of superhydrophobic surfaces by a mussel-inspired polymer coating *Angewandte*  
48 *Chemie International Edition* **49** 9401-4  
49 [52] Young T 1805 III. An essay on the cohesion of fluids *Philosophical Transactions of the Royal*  
50 *Society of London* **95** 65-87  
51 [53] Wenzel R N 1936 Resistance of solid surfaces to wetting by water *Industrial & Engineering*  
52 *Chemistry* **28** 988-94  
53  
54  
55  
56  
57  
58  
59  
60

- 1  
2  
3 [54] Cassie A B D and Baxter S 1944 Wettability of porous surfaces *Transactions of the Faraday*  
4 *society* **40** 546-51
- 5 [55] Afferrante L and Carbone G 2010 Microstructured superhydrorepellent surfaces: effect of  
6 drop pressure on fakir-state stability and apparent contact angles *Journal of Physics:*  
7 *Condensed Matter* **22** 325107
- 8 [56] Afferrante L and Carbone G 2014 The effect of drop volume and micropillar shape on the  
9 apparent contact angle of ordered microstructured surfaces *Soft Matter* **10** 3906-14
- 10 [57] Afferrante L and Carbone G 2015 Statistical theory of wetting of liquid drops on  
11 superhydrophobic randomly rough surfaces *Physical Review E* **92** 042407
- 12 [58] Ciavarella M and Afferrante L 2016 Adhesion of rigid rough contacts with bounded distribution  
13 of heights *Tribology International* **100** 18-23
- 14 [59] Jung M, Brinkmann M, Seemann R, Hiller T, Sanchez de La Lama M and Herminghaus S 2016  
15 Wettability controls slow immiscible displacement through local interfacial instabilities  
16 *Physical Review Fluids* **1** 074202
- 17 [60] Violano G and Afferrante L 2019 Contact of rough surfaces: Modeling adhesion in advanced  
18 multiasperity models *Proceedings of the Institution of Mechanical Engineers, Part J: Journal of*  
19 *Engineering Tribology* **233** 1585-93
- 20 [61] Marmur A and Bittoun E 2009 When Wenzel and Cassie Are Right: Reconciling Local and Global  
21 Considerations *Langmuir* **25** 1277-81
- 22 [62] Bittoun E and Marmur A 2010 Chemical Nano-Heterogeneities Detection by Contact Angle  
23 Hysteresis: Theoretical Feasibility *Langmuir* **26** 15933-7
- 24 [63] Carbone G and Mangialardi L 2005 Hydrophobic properties of a wavy rough substrate *The*  
25 *European Physical Journal E* **16** 67-76
- 26 [64] Bottiglione F and Carbone G 2013 Role of Statistical Properties of Randomly Rough Surfaces  
27 in Controlling Superhydrophobicity *Langmuir* **29** 599-609
- 28 [65] Brown P S and Bhushan B 2016 Designing bioinspired superoleophobic surfaces *APL Materials*  
29 **4** 015703
- 30 [66] Brown P S and Bhushan B 2016 Durable, superoleophobic polymer–nanoparticle composite  
31 surfaces with re-entrant geometry via solvent-induced phase transformation *Scientific reports*  
32 **6** 21048
- 33 [67] Lempešis N, Janka A, Gnatiuk O, van Eijndhoven S J L and Koopmans R J 2020 Predicting bio-  
34 inspired candidate surfaces with superomniphobic characteristics *Surface Topography:*  
35 *Metrology and Properties*
- 36 [68] Vázquez U O M, Shinoda W, Moore P B, Chiu C-c and Nielsen S O 2009 Calculating the surface  
37 tension between a flat solid and a liquid: a theoretical and computer simulation study of three  
38 topologically different methods *Journal of Mathematical Chemistry* **45** 161-74
- 39 [69] Zisman W A 1964 *Contact Angle, Wettability, and Adhesion*: AMERICAN CHEMICAL SOCIETY)  
40 pp 1-51
- 41 [70] Owens D K and Wendt R C 1969 Estimation of the surface free energy of polymers *Journal of*  
42 *Applied Polymer Science* **13** 1741-7
- 43 [71] Ayyoob M and Kim Y J 2018 Effect of Chemical Composition Variant and Oxygen Plasma  
44 Treatments on the Wettability of PLGA Thin Films, Synthesized by Direct Copolycondensation  
45 *Polymers (Basel)* **10** 1132
- 46 [72] Cheng C T, Zhang G and To S 2016 Wetting characteristics of bare micro-patterned cyclic olefin  
47 copolymer surfaces fabricated by ultra-precision raster milling *RSC Advances* **6** 1562-70
- 48 [73] Lv T, Cheng Z, Zhang D, Zhang E, Zhao Q, Liu Y and Jiang L 2016 Superhydrophobic Surface  
49 With Shape Memory Micro/Nanostructure and Its Application in Rewritable Chip for Droplet  
50 Storage *ACS Nano* **10** 9379-86
- 51 [74] Lee S G, Lee D Y, Lim H S, Lee D H, Lee S and Cho K 2010 Switchable Transparency and Wetting  
52 of Elastomeric Smart Windows *Advanced Materials* **22** 5013-7
- 53  
54  
55  
56  
57  
58  
59  
60

- 1  
2  
3 [75] Lin G, Zhang Q, Lv C, Tang Y and Yin J 2018 Small degree of anisotropic wetting on self-similar  
4 hierarchical wrinkled surfaces *Soft Matter* **14** 1517-29  
5 [76] Lee W-K, Jung W-B, Nagel S R and Odom T W 2016 Stretchable Superhydrophobicity from  
6 Monolithic, Three-Dimensional Hierarchical Wrinkles *Nano Letters* **16** 3774-9  
7  
8  
9  
10  
11  
12  
13  
14  
15  
16  
17  
18  
19  
20  
21  
22  
23  
24  
25  
26  
27  
28  
29  
30  
31  
32  
33  
34  
35  
36  
37  
38  
39  
40  
41  
42  
43  
44  
45  
46  
47  
48  
49  
50  
51  
52  
53  
54  
55  
56  
57  
58  
59  
60